ChemSusChem

Supporting Information

Graphitic Carbon Nitride Structures on Carbon Cloth Containing Ultra- and Nano-Dispersed NiO for Photoactivated Oxygen Evolution

Enrico Scattolin, Mattia Benedet, Gian Andrea Rizzi, Alberto Gasparotto, Oleg I. Lebedev, Davide Barreca,* and Chiara Maccato

Supporting Information

for

Graphitic Carbon Nitride structures on Carbon Cloth containing Ultra- and Nano-Dispersed NiO for Photoactivated Oxygen Evolution

Enrico Scattolin,[a] Mattia Benedet,[a],[b] Gian Andrea Rizzi,[a],[b] Alberto Gasparotto,[a],[b]

Oleg I. Lebedev,[c] Davide Barreca,[b],* and Chiara Maccato[a],[b]

[a] Department of Chemical Sciences, Padova University and INSTM, Via Marzolo, 1 - 35131 Padova, Italy.

[b] CNR-ICMATE and INSTM, Department of Chemical Sciences, Padova University, Via Marzolo, 1 - 35131 Padova, Italy.

[c] Laboratoire CRISMAT, UMR 6508 Normandie Université - CNRS, ENSICAEN, UNICAEN, 6, Boulevard Marechal Juin - 14050 Caen, Cedex 4, France.

* Corresponding author. E-mail: davide.barreca@unipd.it.

§ S1. Additional experimental details

§ S1-1 Preparation

Synthesis of gCN powders. In a typical experiment, 2.0 g of melamine (M) and 2.0 g of cyanuric acid (C) were dissolved in 80 mL and 40 mL of dimethylsulphoxide, respectively. After complete solubilization, the cyanuric acid-containing solution was added dropwise to the melamine-containing one. The appearance of a white precipitate was associated to the formation of a CM supramolecular adduct. After stirring for 10 min, the adduct was filtered and washed with two aliquots of ethanol (10 mL each). The powders were then dried in oven at 50°C for 3 h and subsequently heated in air at 550°C for 2:30 h (rate 3°C/min). In the end, an ochre-colored product was collected.

Synthesis of NiO-functionalized gCN powders. The synthesis of NiO-functionalized powders was performed after carefully modifying the procedure proposed by Chebanenko *et al*.[1] Details for the target systems are provided in the following. **Synthesis of gCN/NiO UD powders**. In a typical experiment, instead of using 0.2 g of gCN in 150 mL deionized water, as suggested in the original procedure and subsequently dividing the obtained suspension into three batches, 100 mg of gCN powders were suspended in 75 mL of deionized water by magnetic stirring for 1 h. Subsequently, 0.02 mmol of $Ni(OAc)_2 \cdot 4H_2O$ (Sigma Aldrich, 98%) were added to the suspension, and sonicated for 2 h. The subsequent removal of water took place by gentle heating, instead of setting the temperature to 100°C.[1] Finally the powders were treated in the same conditions as reported (300°C for 30 min in air), but applying a heating rate of 3°C/min. **Synthesis of gCN/NiO ND powders**. gCN/NiO NDH and gCN/NiO NDL powders were prepared following the same procedure described above for gCN/UD, but using 0.03 and 0.01 mmol of $Ni(OAc)_2 \cdot 4H_2O$, respectively.

Synthesis of bare NiO on carbon cloth (CC). The bare NiO sample was prepared as a comparison to specimen gCN/NiO UD, the best performing one. 0.02 mmol of $Ni(OAc)_2 \cdot 4H_2O$ were dissolved in 10 mL acetone (Carlo Erba, ≥ 99.8%). After lying a CC substrate at the bottom of the beaker, the solvent was completely evaporated and the deposit was finally annealed in air at 350°C for 1 h (heating rate = 3°C/min).

§ S1-2 Deposition of bare and NiO functionalized gCN powders on carbon cloth

Before EPD, carbon cloth substrates (≈ 1 × 0.8 cm^2) underwent an accurate cleaning procedure similar to the one employed by Wang *et al.*,[2] but isopropyl alcohol was used instead of ethanol. The cleaning procedure involved three steps:

1. firstly, the carbon cloth was immersed in a beaker containing 50 mL deionized water and sonicated for 5 min. At the end, it was taken out and rinsed with deionized water again;
2. secondly, the carbon cloth was immersed into 50 mL isopropyl alcohol and sonicated for 5 min. After extraction, it was thoroughly washed with the same solvent;
3. finally, the substrate was immersed in acetone and sonicated for 5 min before being taken out, washed, and mounted on the EPD apparatus.

Electrophoretic deposition of gCN and gCN/NiO powders on carbon cloth was performed according to a literature procedure[3]: 40 mg powders were dispersed in 50 ml acetone and 10 mg I_2, and sonicated for 20 min, so as to induce the protonation of bare and NiO-functionalized gCN flakes with H^+ ions according to the following reaction:

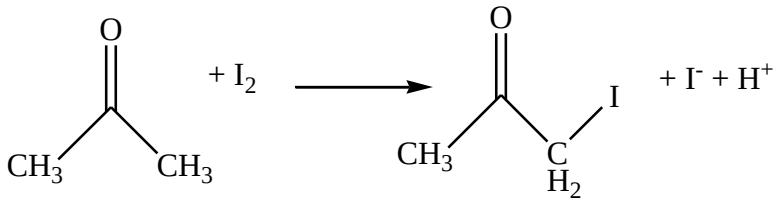

(S1)

In this way, a higher stability of the suspension and a better migration of gCN-based flakes towards the cathode (namely, the negatively-charged carbon cloth) could be obtained, both factors accounting for a higher homogeneity of the resulting deposit.[4] During the EPD process, the carbon cloth and the counter-electrode (a positively-charged graphite stripe) were immersed into the stirred suspension and a constant potential difference of 10 V was applied for 60 seconds. At the end of the deposition, the electrodes were taken out and dried in air. Before chemico-physical and functional characterization, the obtained deposits were annealed in air at 350°C for 1 h (heating rate = 3°C/min).

§ S1-3 Characterization

X-ray diffraction (XRD) measurements were run on a Bruker AXS D8 Advance Plus diffractometer equipped with a CuKα X-ray source (λ = 1.54051 Å) powered at 40 kV and 40 mA. The analysis of gCN-based powders was carried out in a Bragg-Brentano geometry, while CC-supported samples were characterized in a glancing incidence mode (θ_i = 1.0°) configuration. . Analyses were performed at the PanLab facility (Department of Chemical Sciences, Padova University) founded by the MIUR Dipartimento di Eccellenza grant "NExuS".

Photoluminescence (PL) spectra for the carbon cloth-supported materials were collected in the 400−820 nm wavelength range using an FLS 1000 fluorimeter (Edinburgh Instruments). The following settings were used: excitation wavelength/bandwidth = 330/3 nm; emission bandwidth = 5 nm.

Due to the fragility of carbon cloth supports and gCN structures under ion beam irradiation, samples for transmission electron microscopy (TEM) analyses were prepared by careful scratching the target material from the substrate, suspending in ethanol, and final deposition on a TEM grid.

§ S1-4 Electrochemical tests

Current density values (maximum estimated uncertainty = ± 2%) were obtained by dividing the measured currents for the exposed geometric area (≈ 0.8 cm^2). In fact, as already reported, for materials similar to the present ones, BET measurements of the real active area and a reliable evaluation of electrochemical active surface area (ECSA) are not feasible.[5]

The potential values *vs.* Ag/AgCl were converted into the reversible hydrogen electrode (RHE) scale using the relation:

$$E_{RHE}\ (V) = E_{Ag/AgCl}\ (V) + 0.0592 \times pH + 0.199 \qquad (S2)$$

where $E_{Ag/AgCl}$ stands for the bias applied between the working and counter electrodes. Linear sweep voltammetry (LSV) curves were collected in the interval 0.65 to 1.75 V_{RHE}.

Electrochemical impedance spectroscopy (EIS) experiments were carried out between 1 and 10^5 Hz with a 5 mV perturbation.

§ S2. Chemico-physical characterization

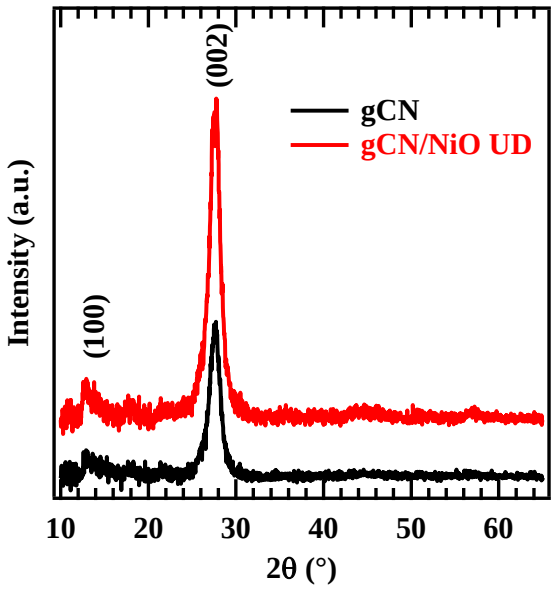

Figure S1. Representative XRD patterns recorded on gCN and gCN/NiO UD powders. The signals at 2θ ≈ 13.1° and 27.3° were attributed to the packing of tri-s-triazine units in (100) crystallographic planes and to the (002) interplanar stacking of gCN sheets, respectively.[5-6] Evaluation of the average crystallite dimensions by the Scherrer formula yielded values of (6±1) nm for both specimens. No diffraction peak attributable to NiO could be identified, due to the high dispersion and small size of NiO particles in gCN matrices.

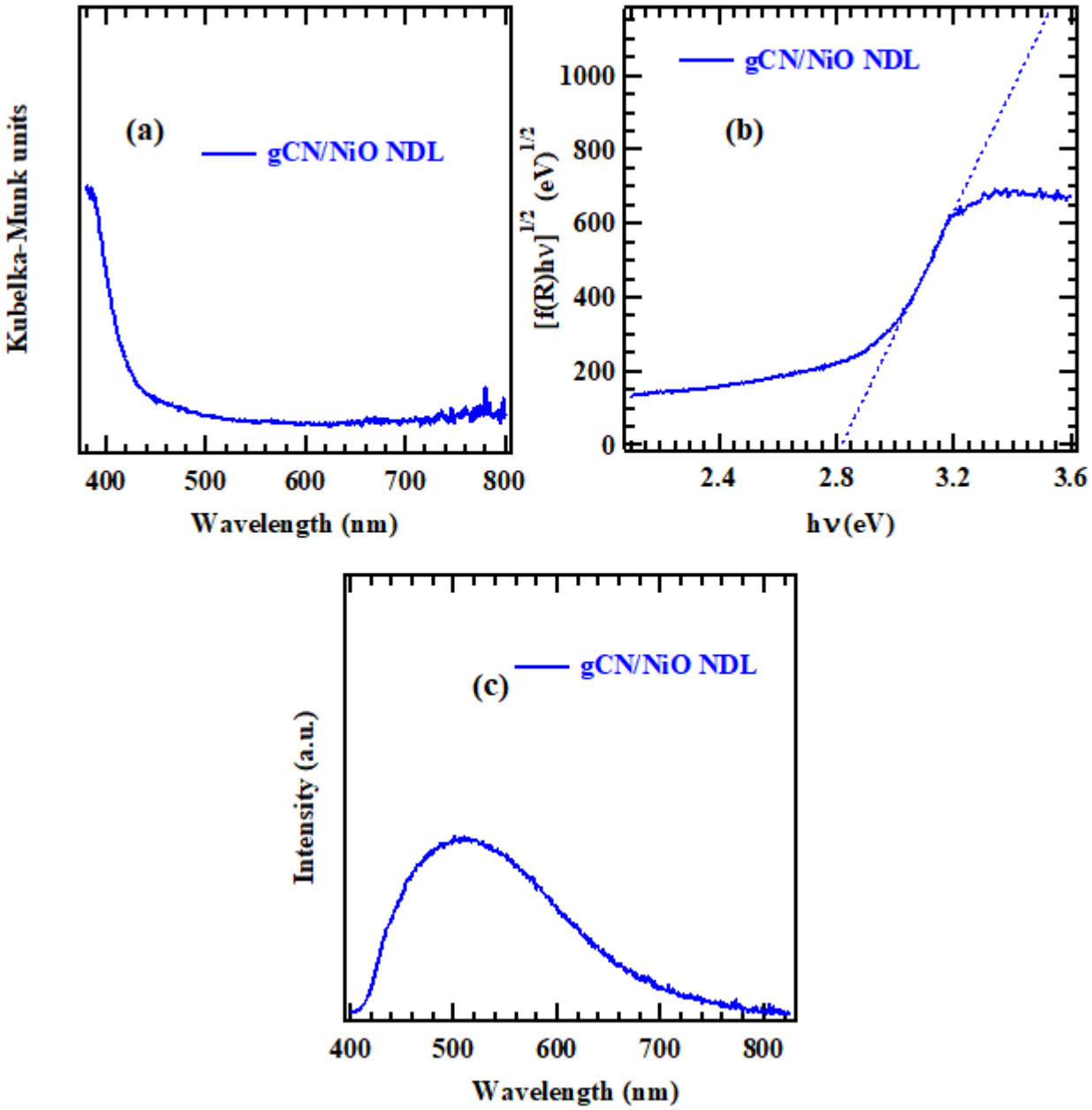

Figure S2. Optical spectrum (a), Tauc plot (b) and PL spectrum (c) of carbon cloth-supported gCN/NiO NDL.

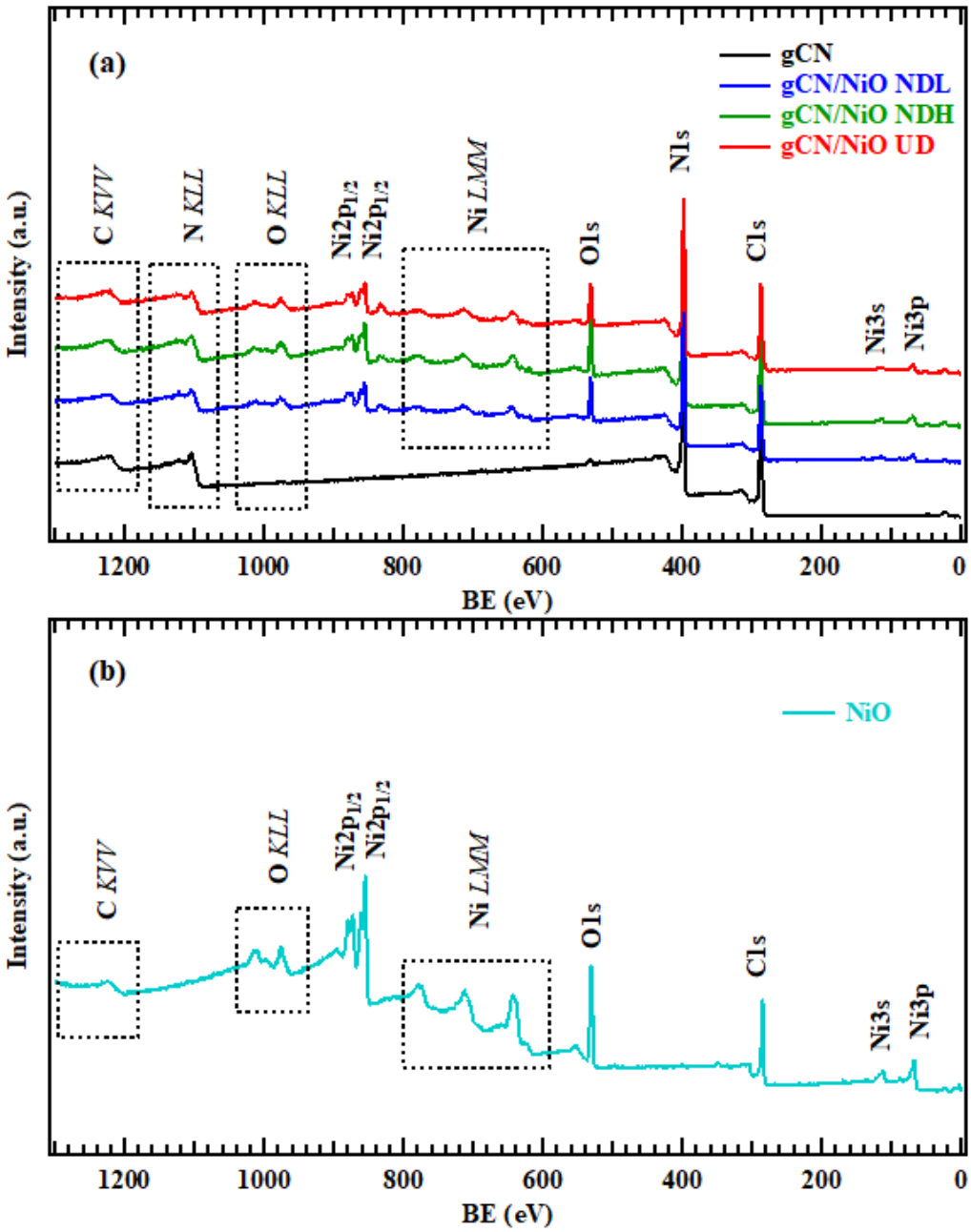

Figure S3. X-ray photoelectron spectroscopy (XPS) wide-scan spectra for: (a) bare and NiO-containing gCN electrocatalysts; (b) a reference nickel oxide sample, supported on carbon cloth.

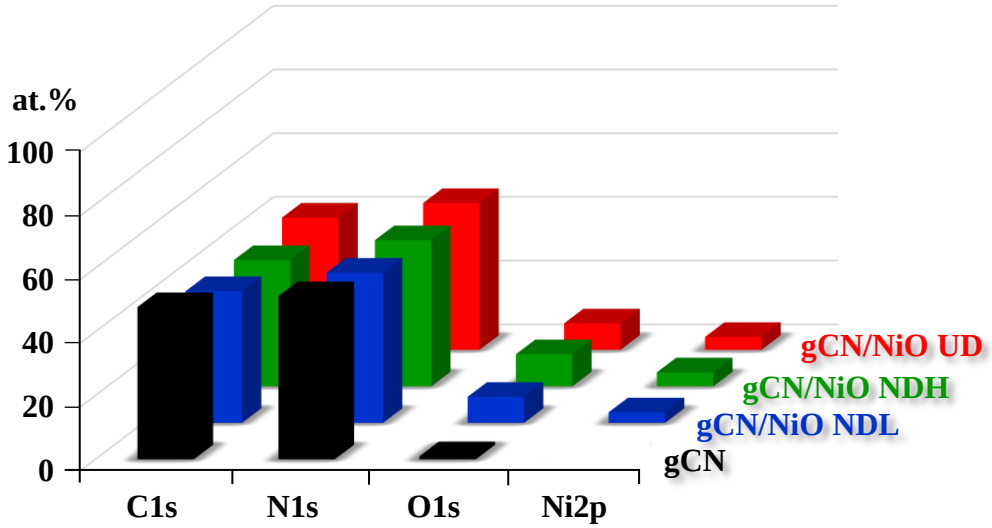

Figure S4. Atomic percentage (at. %) data obtained by XPS analyses for gCN and gCN/NiO electrocatalysts.

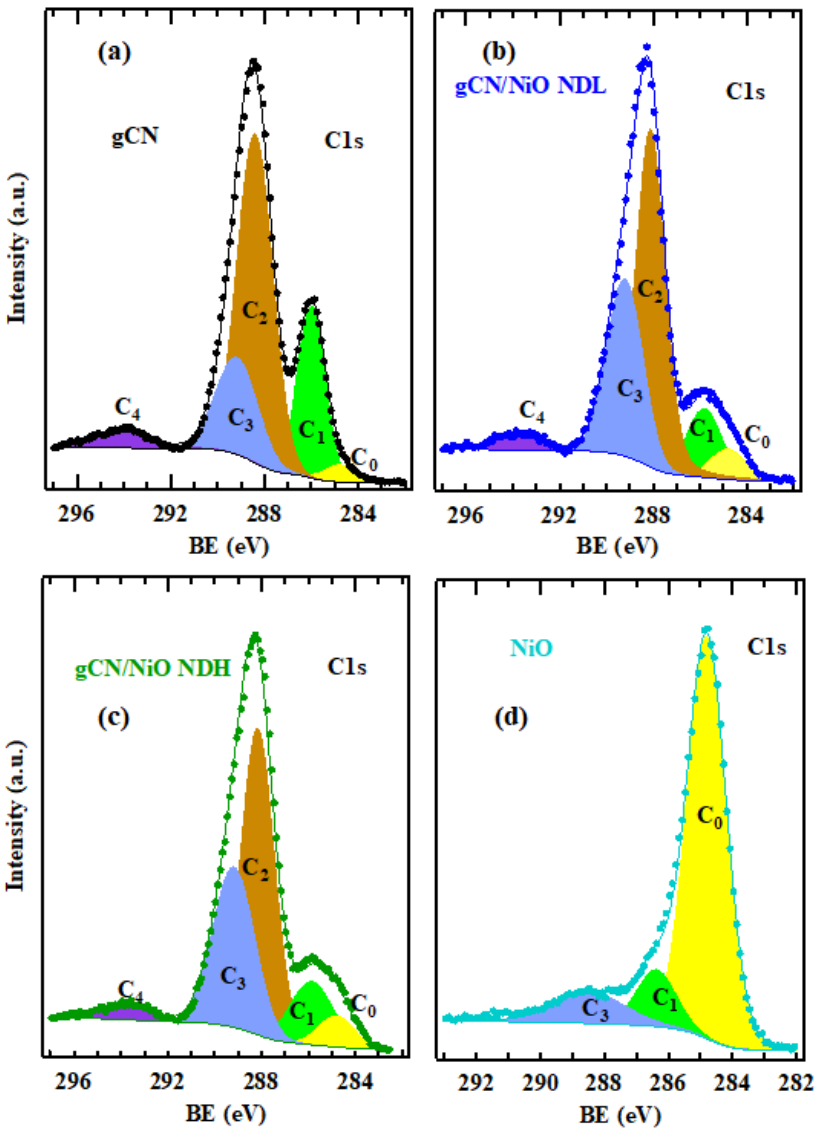

Figure S5. C1s photoelectron peaks for gCN, gCN/NiO NDL, gCN/NiO NDH and NiO electrocatalysts.

Sample	C_0		C_1		C_2		C_3		C_4	
	BE (C_0) (eV)	% (C_0)	BE (C_1) (eV)	% (C_1)	BE (C_2) (eV)	% (C_2)	BE (C_3) (eV)	% (C_3)	BE (C_4) (eV)	% (C_4)
gCN	284.8	2.6	286.0	23.0	288.4	51.9	289.2	18.2	294.0	4.3
gCN/NiO UD	284.8	10.6	285.7	8.1	288.0	55.9	289.1	20.7	293.7	4.7
gCN/NiO NDL	284.8	5.0	285.9	11.3	288.2	50.3	289.2	30.0	293.9	3.4
gCN/NiO NDH	284.8	5.2	285.8	12.3	288.1	48.8	289.2	30.4	293.8	3.3
NiO	284.8	77.6	286.4*	11.3	--	--	288.4	11.1	--	--

Table S1. Binding energy (BE, eV) and relative contribution (%) of the various C1s components to the overall C1s signal for the indicated specimens. Color codes as in Figures 3a and S5. Component C_0 appears to be significantly weaker for the composite samples with respect to bare NiO, due to a higher coverage degree of the carbon cloth substrate in the former case.

* For bare NiO, the C_1 signal was associated to the presence of C-O-C and C-O-H groups of the uncovered carbon cloth substrate, arising from exposure to air and moisture.[7]

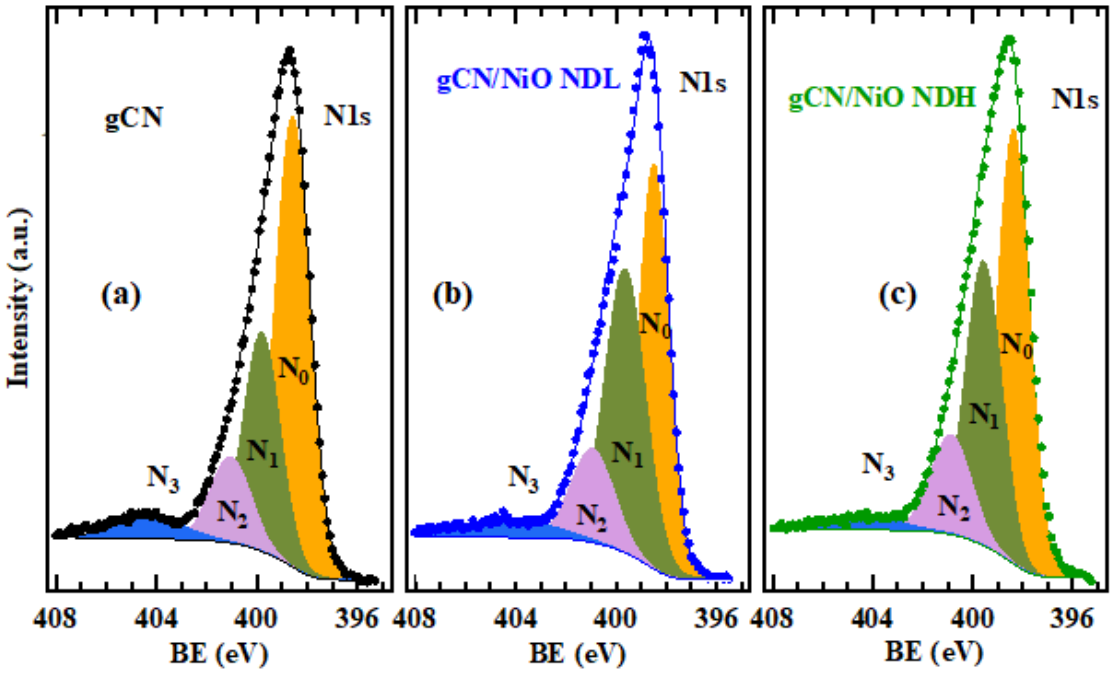

Figure S6. N1s photoelectron peaks for gCN, gCN/NiO NDL and gCN/NiO NDH electrocatalysts.

Sample	N_0		N_1		N_2		N_3	
	BE (N_1) (eV)	% (N_1)	BE (N_2) (eV)	% (N_2)	BE (N_3) (eV)	% (N_3)	BE (N_4) (eV)	% (N_4)
gCN	398.6	53.5	399.8	28.6	401.2	12.2	404.2	5.7
gCN/NiO UD	398.3	62.4	399.5	23.9	400.9	7.9	403.9	5.8
gCN/NiO NDL	398.5	41.2	399.7	39.9	401.1	13.9	404.1	5
gCN/NiO NDH	398.4	48.0	399.6	34.7	401.0	14.2	404.0	3.1

Table S2. BE (eV) and relative contribution (%) of the various N1s components to the overall N1s signal for the indicated specimens. Color codes as in Figures 3b and S6.

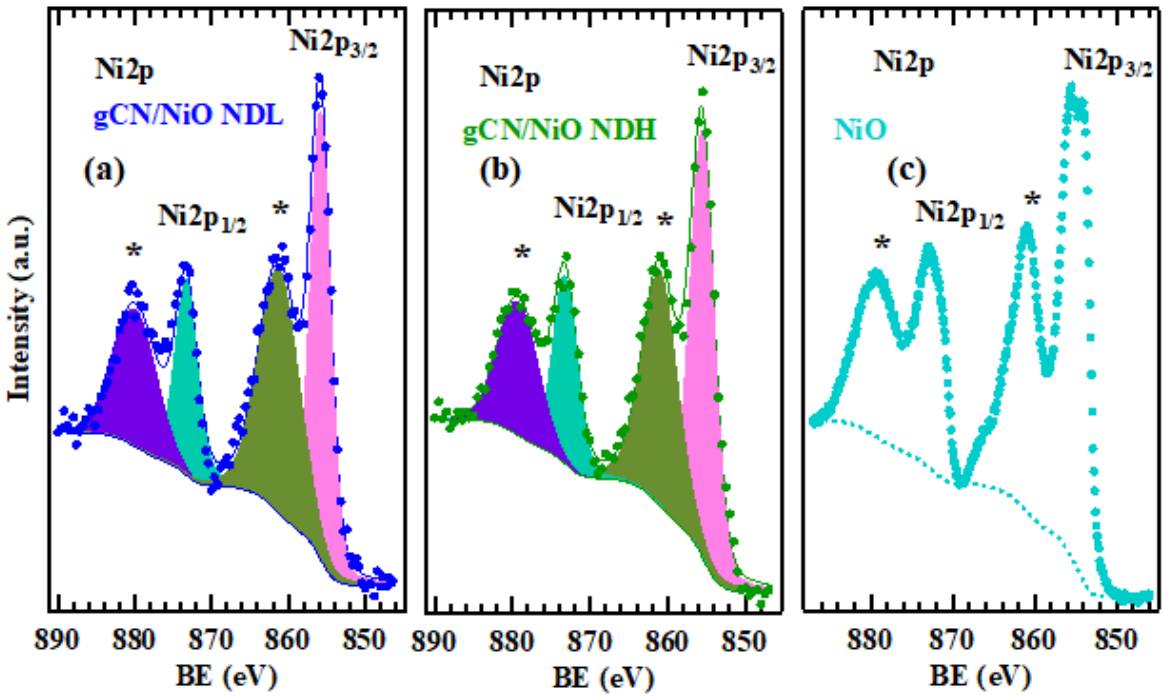

Figure S7. Ni2p photoelectron signals for gCN/NiO NDL, gCN/NiO NDH and bare NiO specimens. Satellite peaks are marked by *.

Sample	$Ni2p_{3/2}$	$Ni2p_{3/2}$ satellite	$Ni2p_{1/2}$	$Ni2p_{1/2}$ satellite
	BE (eV)	BE (eV)	BE (eV)	BE (eV)
gCN/NiO UD	855.1	861.0	872.9	879.3
gCN/NiO NDL	855.4	861.1	873.2	879.4
gCN/NiO NDH	855.5	861.2	873.3	879.5
NiO	854.9	860.9	872.7	879.2

Table S3. BE (eV) of Ni2p spin-orbit components and pertaining satellites for the indicated samples. Color codes as in Figures 3c and S7a-b. For bare NiO specimen, the $Ni2p_{3/2}$ position is referred to the most intense component located at the lowest BE.

To attain a detailed understanding of the Ni2p photopeak shape, heavily dependent on the multi-electronic interactions with closest neighbors of the emitting atom,[8] it is worth recalling that NiO is a charge transfer oxide whose fundamental state results from the following contributing configurations: $3d^8$, $3d^9\underline{L}$ and $3d^{10}\underline{L}^2$, where $\underline{L}$ indicates a hole in the oxygen site bound to the Ni emitting centre.[9] As regards the $Ni2p_{3/2}$ and its satellite for all samples (Figures 3c and S7), it is widely accepted that the signal at ≈ 861.0 eV corresponds to the $3d^{10}\underline{L}^2$ and $\underline{c}3d^8$ configurations, whereas the more intense peak at ≈ 855.0 eV is ascribed to the $\underline{c}3d^9\underline{L}$ one, with $\underline{c}$ representing a hole in the Ni2p core level.

As can be observed in Figures 3c-S7 and Table S3, upon passing from bare NiO to gCN/NiO specimens, variations in the shape and position of the Ni2p peak take place, in line with previous results for analogous NiO nanostructured systems.[9-10] In particular, the main signal at ≈ 854.9 eV and the band at ≈ 1.5 eV higher are not resolved, and generate a single structure positioned at higher BEs with respect to the bare NiO reference specimen. An analogous behaviour has been observed upon passing from NiO thin films to dispersed nanoparticles,[9] and for NiO quantum dots/nanoparticles in gCN composite systems.[11] Accordingly, the present Ni2p photopeak variations can be traced back to the high dispersion of low-sized NiO nanoaggregates into the hosting gCN matrix, as supported by morphological analysis results (see Figures 4-6 and related observations in the main manuscript text).

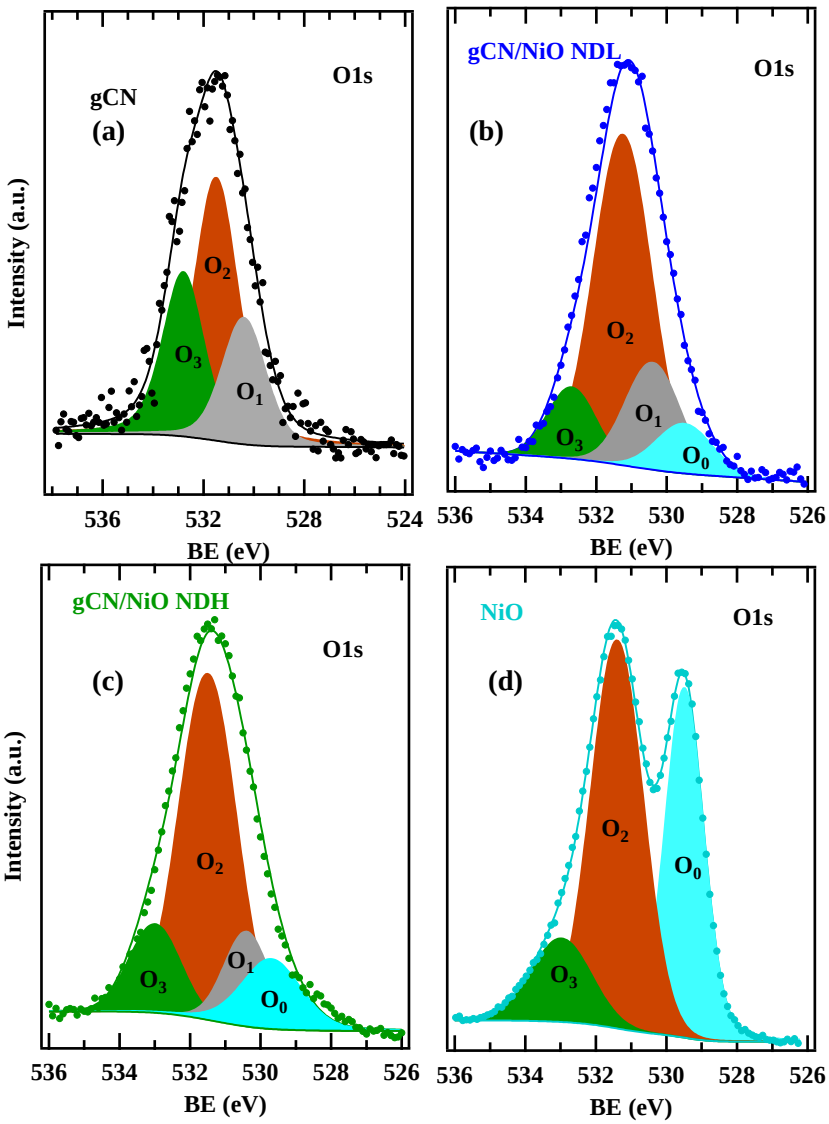

Figure S8. O1s photoelectron peaks for the indicated electrocatalysts.

Sample	O_0		O_1		O_2		O_3	
	BE (O_0) (eV)	% (O_0)	BE (O_1) (eV)	% (O_1)	BE (O_2) (eV)	% (O_2)	BE (O_3) (eV)	% (O_3)
gCN	--	--	530.4	22	531.5	49.2	532.8	28.8
gCN/NiO UD	529.6	18.4	530.4	33	531.5	38.8	533.0	9.8
gCN/NiO NDL	529.7	8.9	530.4	18.8	531.5	61.2	533.0	11.1
gCN/NiO NDH	529.8	13.7	530.4	13.4	531.5	59.3	533.0	13.6
NiO	529.5	36.3	--	--	531.4	51.2	533.0	12.5

Table S4. BE (eV) and relative contribution (%) of the various O1s components to the overall O1s signal for the indicated specimens. Color codes as in Figures 3d and S8.

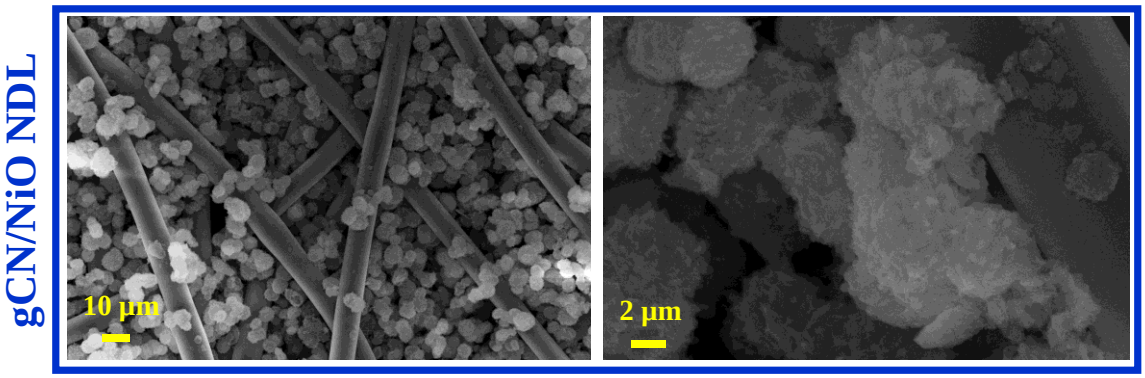

Figure S9. Representative field emission-scanning electron microscopy (FE-SEM) micrographs for gCN/NiO NDL electrocatalyst.

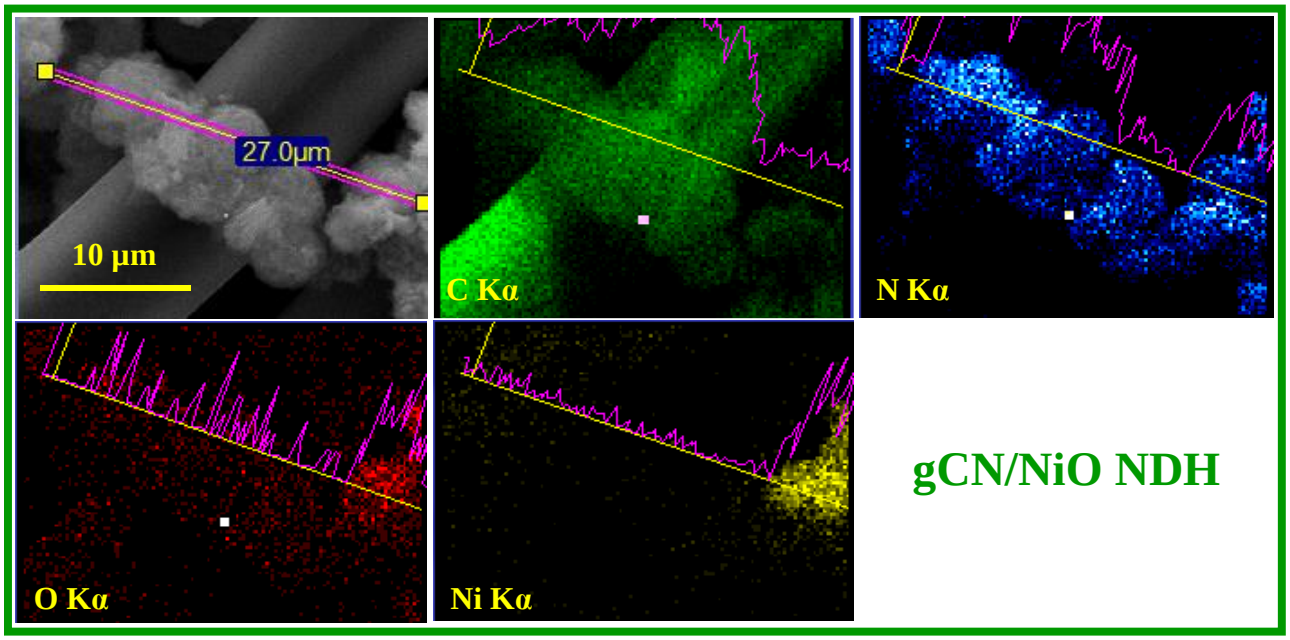

Figure S10. Energy dispersive X-ray spectroscopy (EDXS) elemental maps for gCN/NiO NDH electrocatalyst, with superimposed the elemental scan along the line marked in the electron image in top left panel.

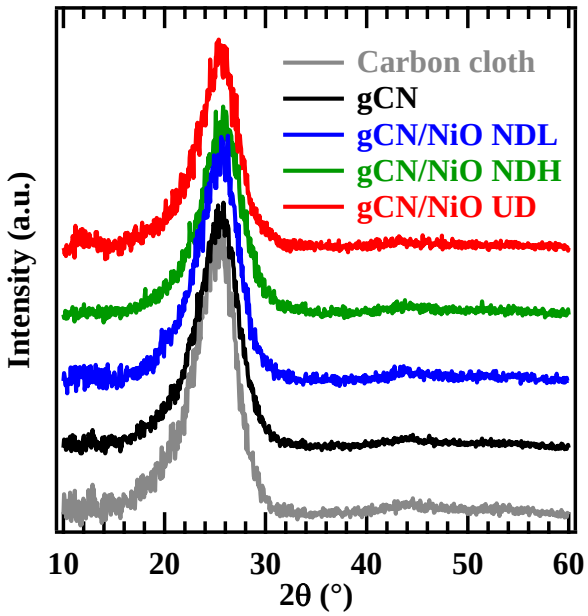

Figure S11. XRD patterns recorded in glancing incidence mode (θ_i = 1.0°) on CC-supported gCN-containing electrocatalysts and the carbon cloth substrate. The broad signal centered at 2θ = 25.5° is mainly ascribed to the (002) plane of graphite carbon in the substrate,[2, 12] even though a possible contribution in the functionalized specimens may arise from carbon nitride presence (compare with Figure S1).

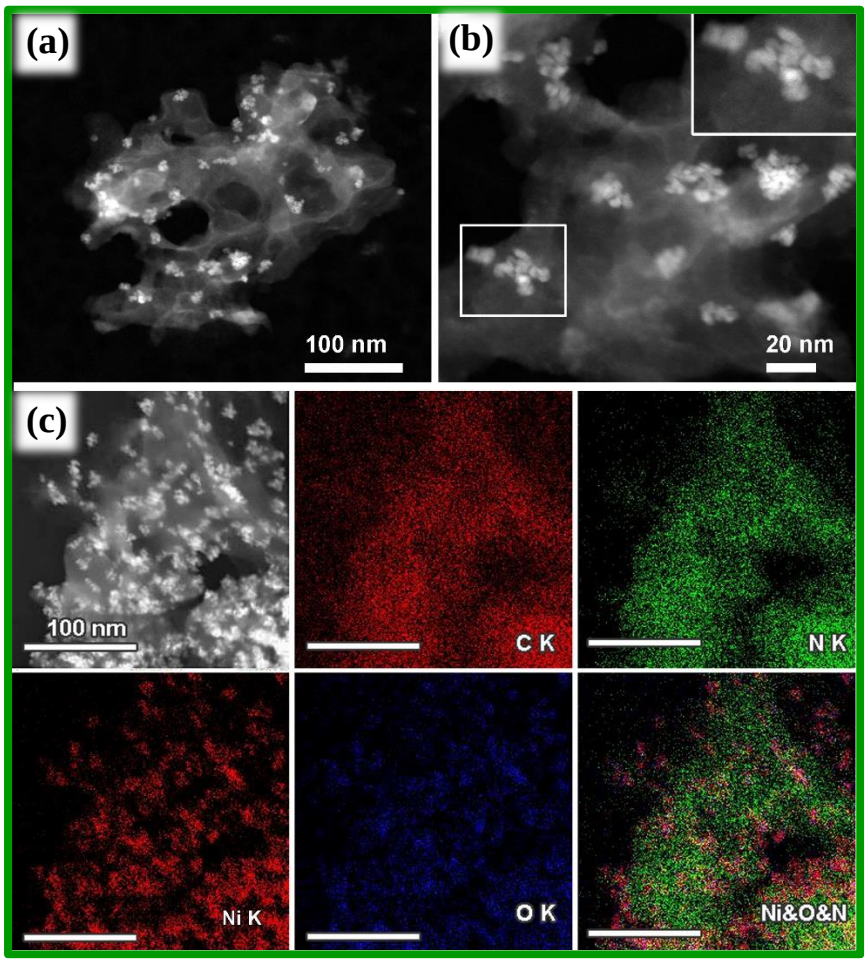

Figure S12. (a) Low magnification high angle annular dark field-scanning TEM (HAADF-STEM) image of gCN/NiO NDH. (b) HAADF-STEM image of NiO nanoparticle agglomerates. A selected NiO agglomerate area (white rectangle) is displayed as inset. (c) Low magnification HAADF-STEM image, corresponding STEM-EDXS chemical maps for C Kα, N Kα, Ni Kα, O Kα, and superimposed color image.

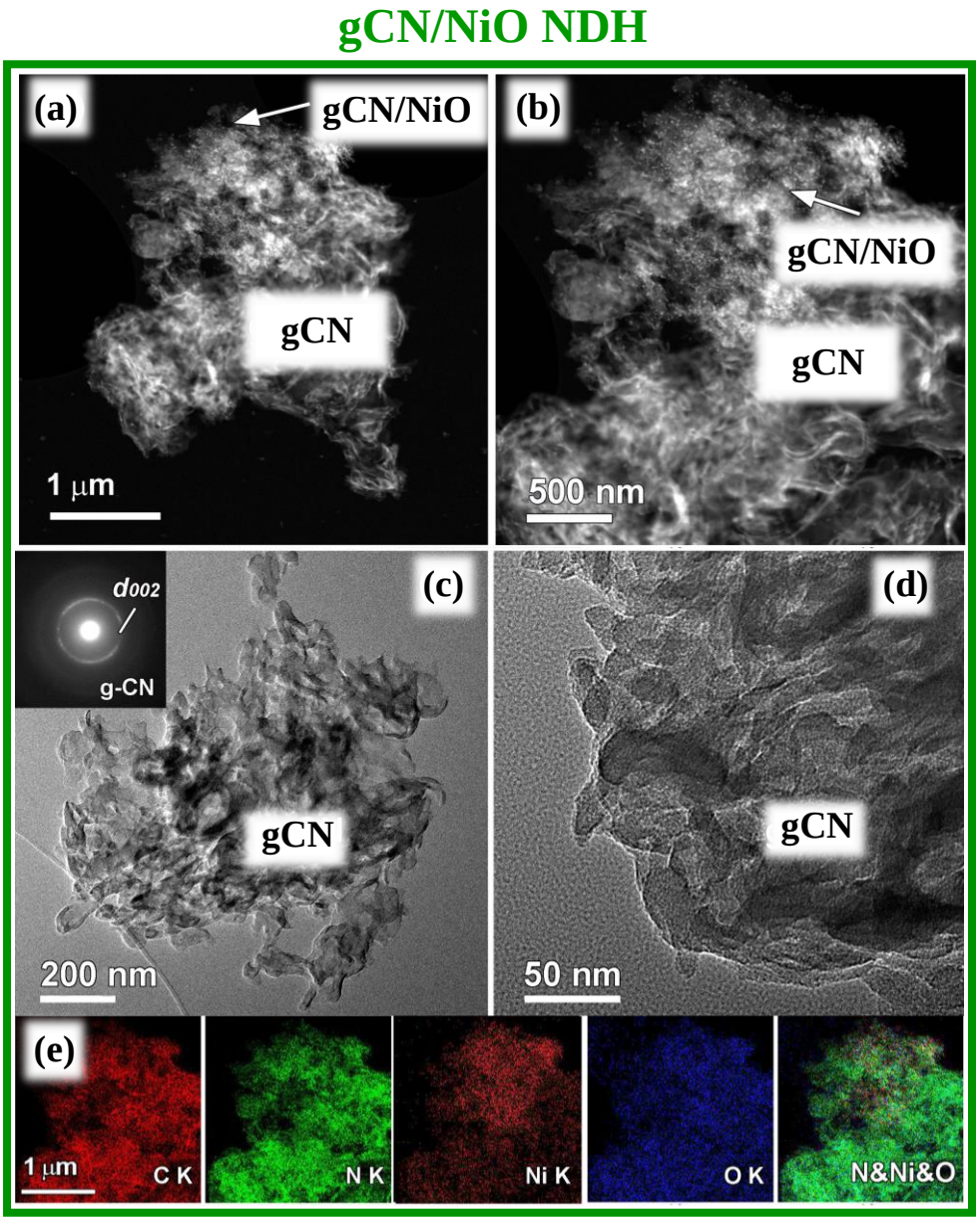

Figure S13. Low magnification (a) and magnified (b) HAADF-STEM images, and (c) low magnification bright field (BF)-TEM image of gCN and corresponding selected area electron diffraction (SAED) pattern for sample gCN/NiO NDH. The characteristic gCN d_{002} ring is indexed (interplanar spacing $d_{002} \approx 0.32$ nm). (d) High resolution gCN BF-TEM image. (e) Corresponding EDXS-STEM elemental maps for gCN/NiO NDH. The inner regions correspond to bare gCN, whereas the outermost regions contain both gCN and NiO.

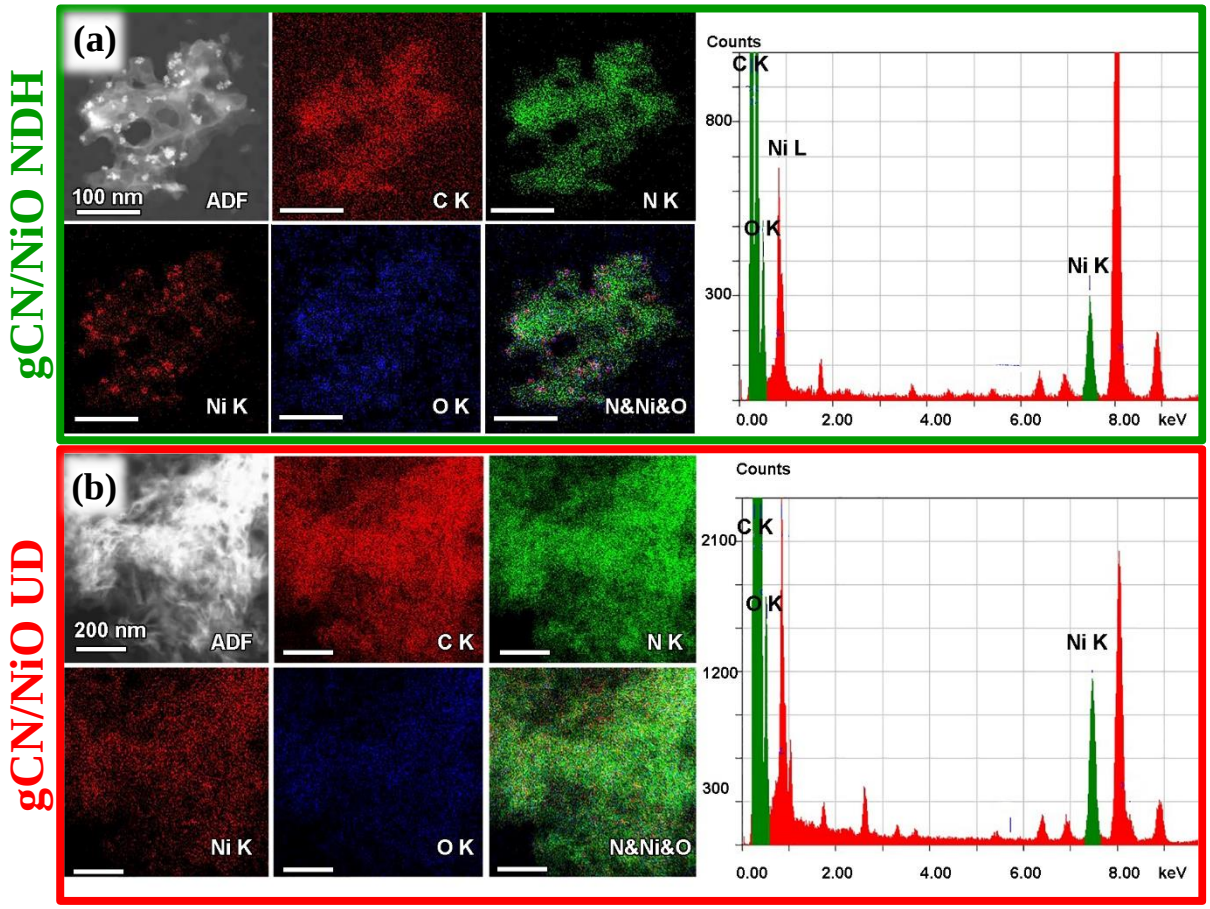

Figure S14. HAADF-STEM images for gCN/NiO NDH (a) and gCN/NiO UD (b), and pertaining EDXS elemental maps. The corresponding EDXS spectra (right side) display in both cases well-detectable Ni signals.

§ S3. Electrochemical tests and related analyses

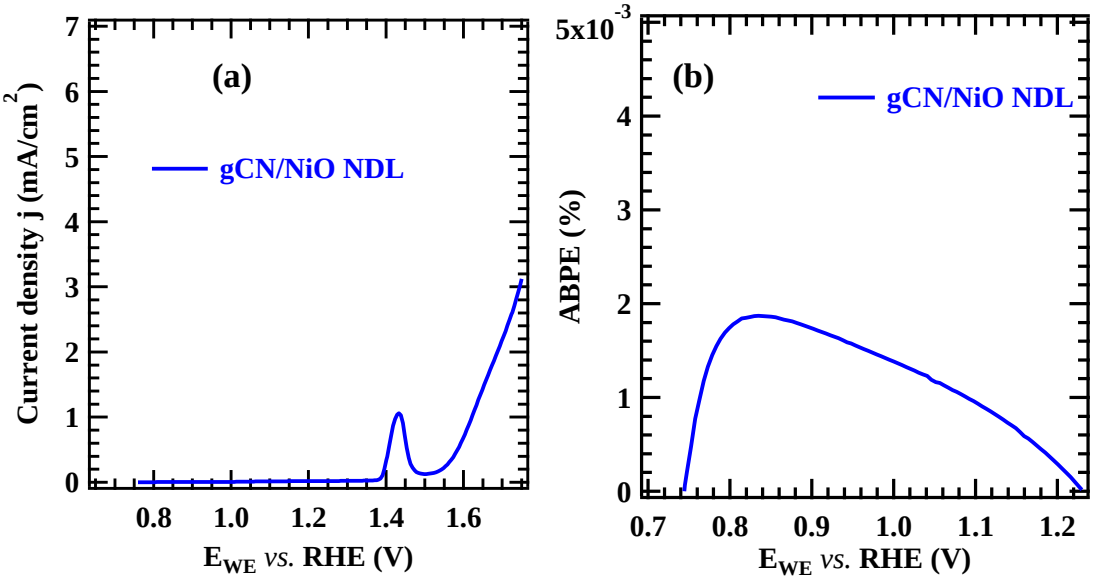

Figure S15. (a) LSV curve registered under illumination and (b) applied bias photon-to-current efficiency (ABPE) % curve for gCN/NiO NDL in 0.1 M KOH.

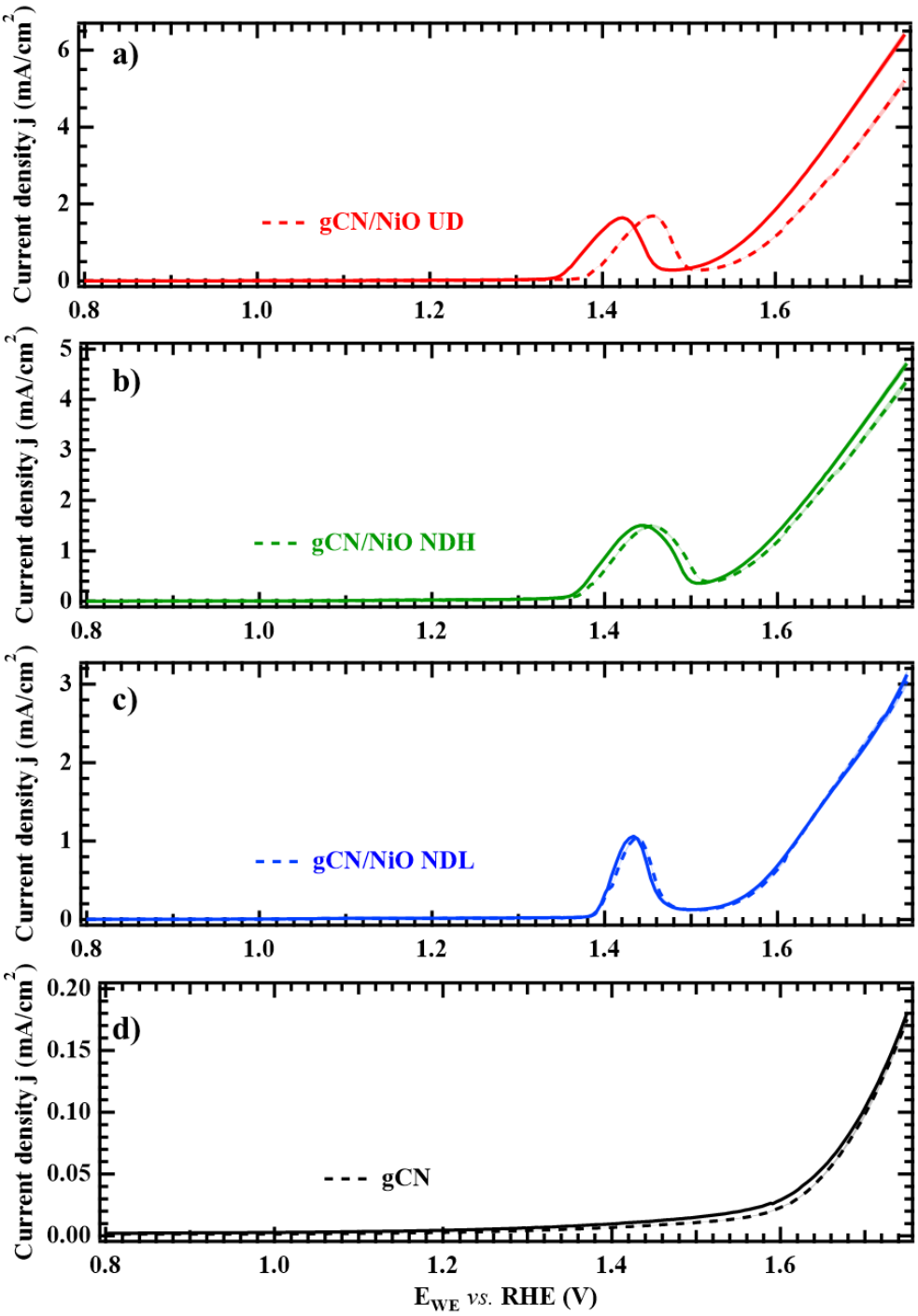

Figure S16. LSV curves recorded in 0.1 M KOH in the dark (dashed lines) and upon illumination (continuous lines) for: (a) gCN; (b) gCN/NiO NDL; (c) gCN/NiO NDH; (d) gCN/NiO UD.

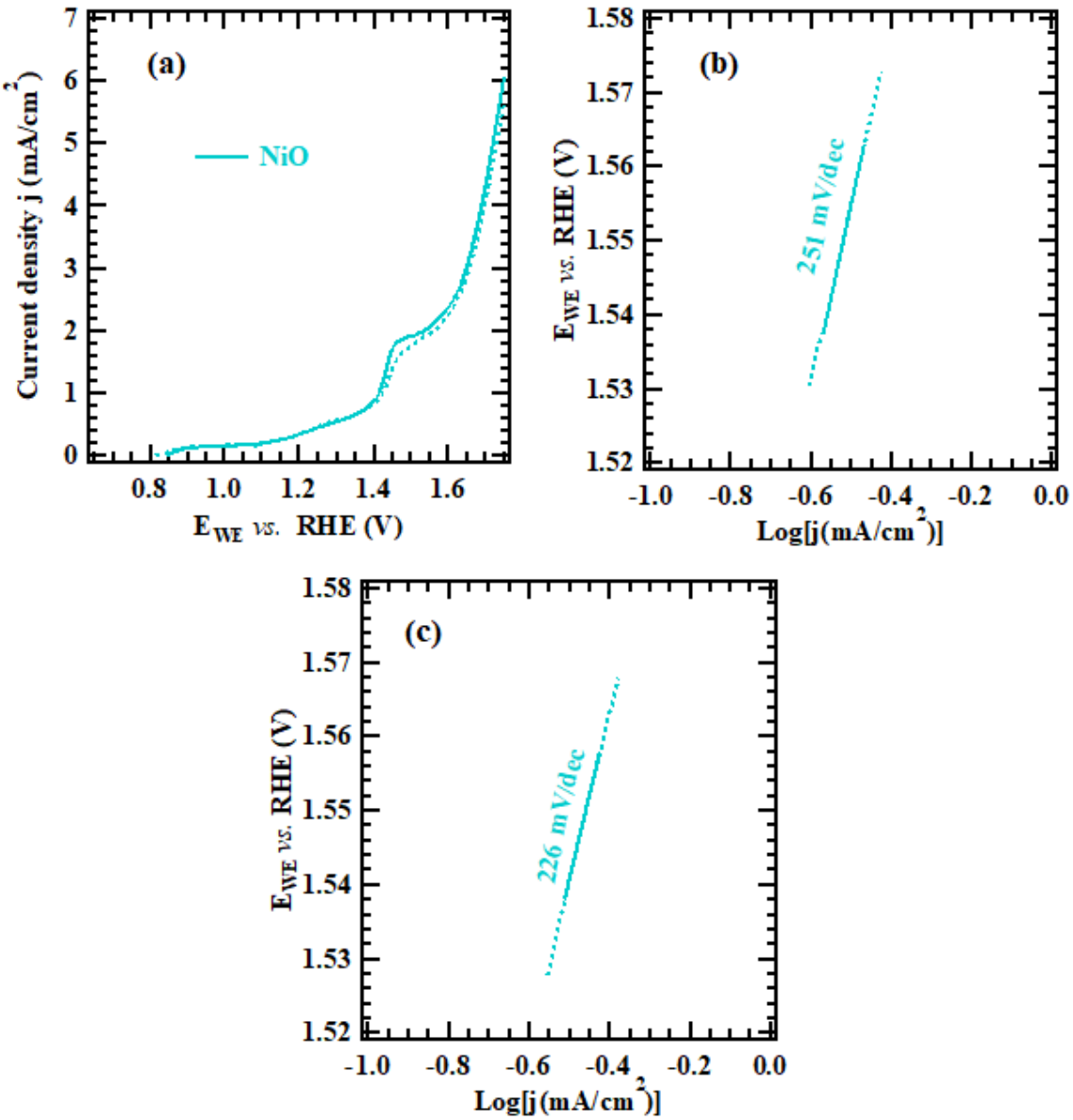

Figure S17. (a) LSV curves registered under illumination (continuous line) and in the dark (dashed line) for bare NiO supported on carbon cloth. Tafel plot in the dark (b) and under illumination (c) for the same specimen. The data have been obtained utilizing 0.1 M KOH as electrolyte.

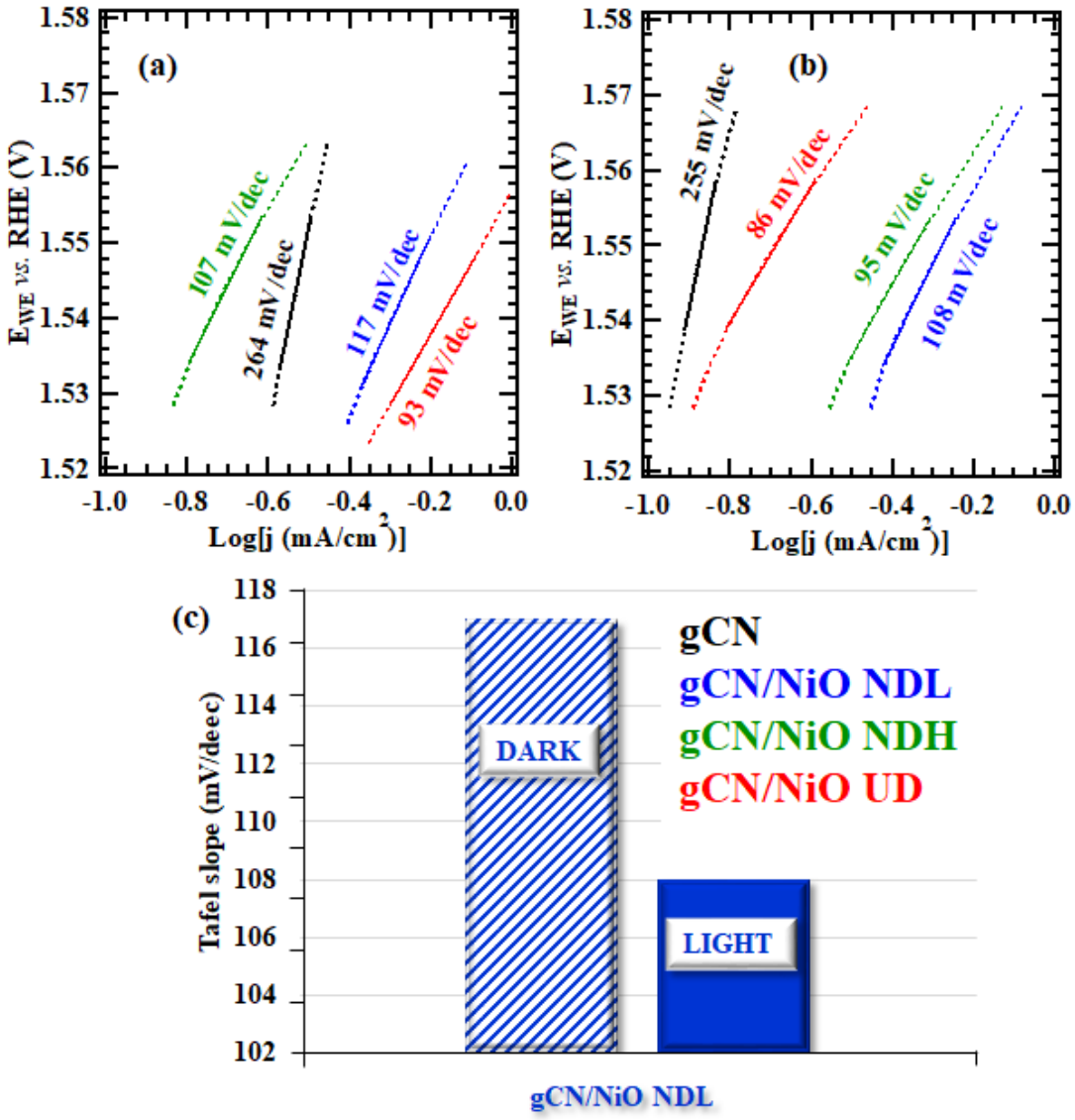

Figure S18. Tafel plots in the dark (a) and under illumination (b) for the target electrocatalysts [sample color codes in panel (c)]. For gCN/NiO NDL, the slope values are also reported in the bar plot of panel (c) (compare with Figure 7b).

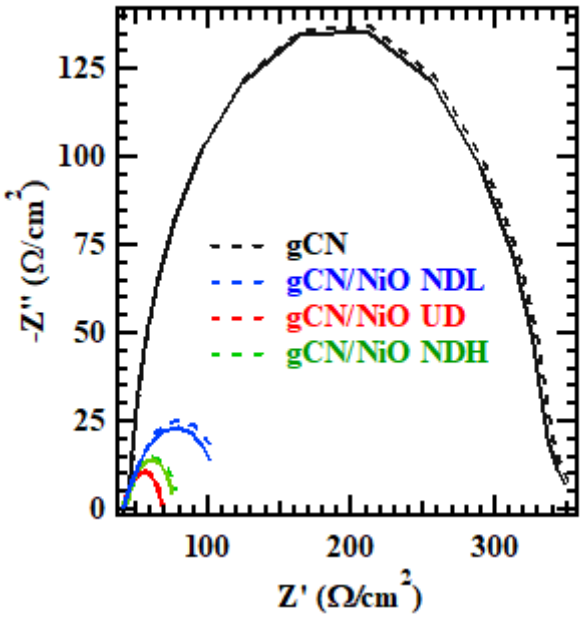

Figure S19. Impedance spectra, reported as Nyquist plots, for bare gCN and gCN/NiO electrocatalysts, recorded in 0.1 M KOH at 1.60 V *vs*. RHE.

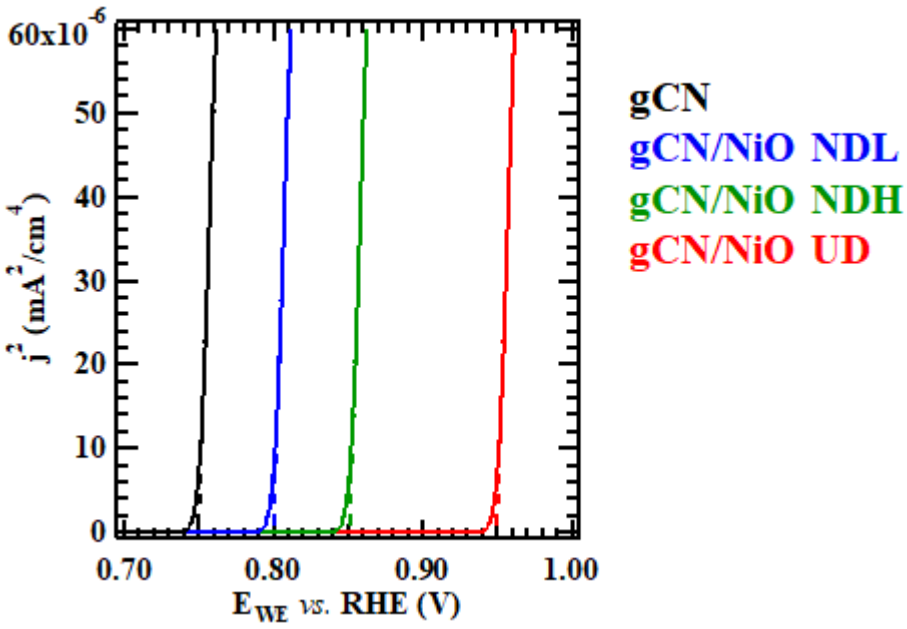

Figure S20. Square photocurrent density (j^2) *vs.* applied bias for the extrapolation of Fermi level potentials through the intercept with the potential axis.[5, 13]

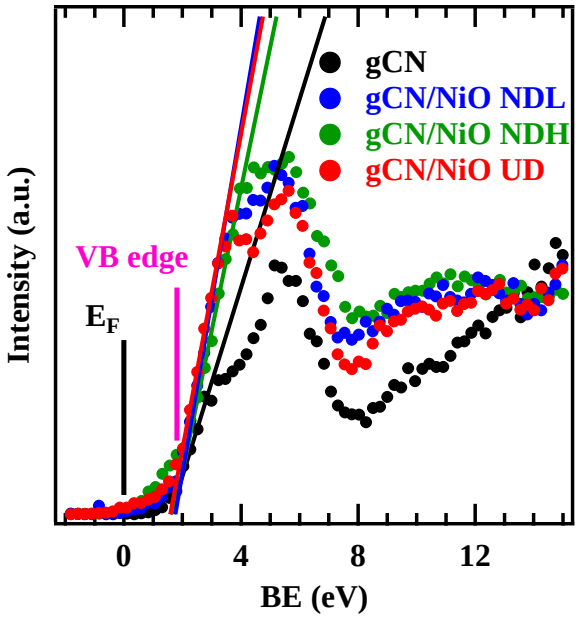

Figure S21. XPS valence band spectra for the indicated specimens (E_F = Fermi level energy; VB = valence band).

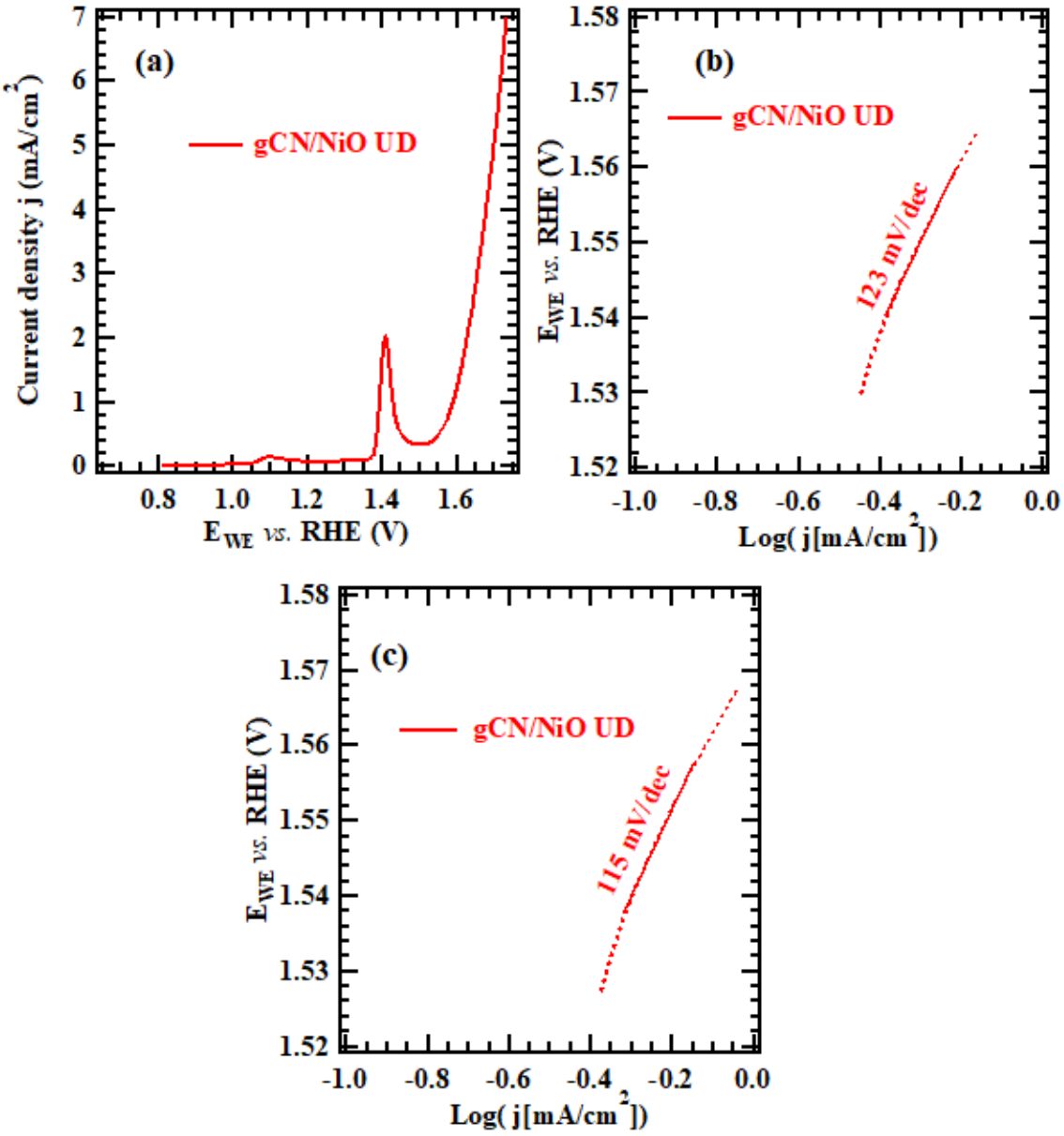

Figure S22. (a) LSV curve registered in the dark for gCN/NiO UD. Tafel plots in the dark (b) and under illumination (c) for the same electrocatalyst. The data were obtained utilizing as electrolyte Adriatic alkaline seawater (pH = 13.58).

Material	Electrolyte	$j_{1.65}$ (mA/cm^2)	E_{onset} (V_{RHE})	$ABPE_{max}$	E_{Wmax} (V_{RHE})
gCN	KOH 0.1 M	0.05	1.55	1.0	0.85
gCN/NiO NDL		1.42	1.28	1.31	0.84
gCN/NiO NDH		2.40	1.23	2.19	0.82
gCN/NiO UD		3.24	1.15	2.75	0.81
gCN/NiO UD	Adriatic alkaline seawater (pH = 13.58)	3.12	1.19	2.69	0.89

Table S5. Summary of representative photoelectrochemical test results for bare gCN and gCN/NiO specimens: photocurrent densities at E = 1.65 V ($j_{1.65}$) *vs.* RHE, onset potential (E_{onset}, calculated at 0.02 mA/cm^2),[14] relative ABPE maximum ($ABPE_{max}$) normalized with respect to bare gCN, and potential of maximum efficiency (E_{Wmax}) corresponding to the maximum in ABPE curves (Figures 7c, S15b, and 9b).

LIGHT			
Material	**Electrolyte**	**Tafel slope (mV/dec)**	**Ref.**
NiO	KOH 0.1 M	226	Present work
gCN		255	
gCN/NiO NDL		108	
gCN/NiO NDH		95	
gCN/NiO UD		86	
gCN/NiO UD	Adriatic alkaline seawater (pH = 13.58)	115	
DARK			
NiO	KOH 0.1 M	251	Present work
gCN		264	
gCN/NiO NDL		117	
gCN/NiO NDH		107	
gCN/NiO UD		93	
gCN/NiO UD	Adriatic alkaline seawater (pH = 13.58)	123	

Table S6. Tafel slope values for the systems fabricated in the present study under illumination and in the dark.

Sample	Electrolyte	$j_{1.65}$ (mA/cm^2)	Tafel slope (mV/dec)	Ref.
gCN	$HClO_4$ (pH = 3)	$< 10^{-4}$ [a]	*n.a.*	[15]
gCN	Na_2SO_4 0.2 M	0.015 [b]	*n.a.*	[16]
gCN	Na_2SO_4 0.2 M	0 [a]	*n.a.*	[17]
gCN	KOH 1.0 M	$\approx 9.0\times10^{-3}$ [b]	*n.a.*	[6a]
gCN	KOH 1.0 M	0 [b]	122	[18]
gCN	KOH 1.0 M	≈ 0.05 [a]	230	[19]
gCN	NaOH 0.1 M	≈ 0.02 [b]	*n.a.*	[20]
NiO-CN$_x$ [c]	Na_2SO_4 0.5 M (pH = 6)	$\approx 3\times10^{-4}$ [b,d]	*n.a.*	[21]
NiO-gCN	NaOH 1.0 M	≈ 17 ÷ ≈ 38 [a]	65	[22]
gCN@NiO	KOH 0.1 M	≈ 0.7 ÷ ≈5.0 [b]	85 ÷ 105	[23]
Ni(OH)$_2$/gCN	NaOH 0.1 M	≈ 0.03 ÷≈ 0.04 [b]	*n.a.*	[20]
Ni(OH)$_2$/gCN	KOH 1.0 M	≈ 4.3 [a]	107	[24]
Ni-Fe-O/gCN [f]	$HClO_4$ (pH = 3)	$\approx 3.5\times10^{-4}$ [a]	*n.a.*	[15]
1% Ni^{2+}-CN$_x$ [c,g]	KOH 0.1 M	≈ 0.30 [b]	*n.a.*	[25]
Ni^{2+}-gCN [g]	KOH 1.0 M	≈ 0.12 ÷ ≈ 0.55 [a]	60 ÷ 88	[19]
TiO$_2$-Ni^{2+}-CN$_x$ [c,g]	Na_2SO_4 0.5 M (pH = 6)	≈ 0.07 [b,d]	*n.a.*	[21]
TiO$_2$-gCN/NiO$_x$	0.1 M borate solution (pH = 7.0)	≈ 0.34 [b,d]	*n.a.*	[26]

Table S7. OER electrochemical performances of selected electrocatalysts based on carbon nitride systems, both as such, combined with NiO or $Ni(OH)_2$, and incorporating Ni centers. *n.a.* = not available. [a] dark conditions; [b] light conditions; [c] CN_x = polymeric carbon nitride; [d] = @ 1.23 eV *vs*. RHE - values at bias > 1.3 V not available; [e] aCN = amorphous carbon nitride; [f] Ni-Fe-O = mixed nickel-iron oxides; [g] atomically dispersed nickel-containing sites.

Material	Electrolyte	$j_{1.65}$ (mA/cm^2)	Tafel slope (mV/dec)	Ref.
IrO_2	1.0 M KOH	18.0	149	[27]
IrO_2	1.0 M KOH	53.0	91	[28]
IrO_2	0.1 M KOH	8.0	113	[29]
IrO_2	1.0 M KOH	1.7	86	[19]
IrO_2	1.0 M KOH	27.0	67	[30]
RuO_2		15.0	89	
RuO_2	1.0 M KOH	13.0	74	[31]
RuO_2	0.1 M KOH	17.0	71	[32]
RuO_2	0.1 M KOH	15.0	198	[33]

Table S8. OER performances of selected IrO_2 and RuO_2 electrocatalysts under dark conditions.

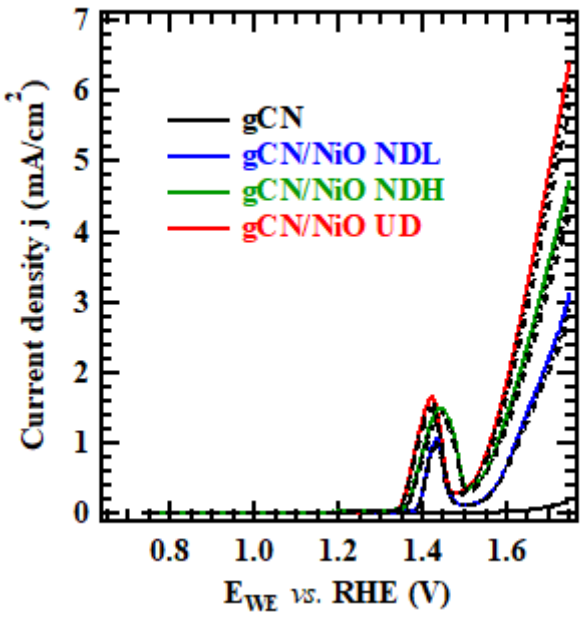

Figure S23. LSV curves recorded under illumination in 0.1 M KOH on as-prepared specimens (solid lines) and collected every 90 days for six months upon sample storage under ambient conditions (dashed lines).

§ S4. Material characterization after photoelectrochemical tests

In order to investigate the stability of the composite materials, post operando XPS analyses have been performed after photoelectrochemical tests in 0.1 M KOH and alkaline seawater (Figure S24), for the best-performing sample, namely gCN/NiO UD. As can be observed, no appreciable variations of any photoelectron peaks were observed with respect to the analyses performed on the as-prepared samples, giving similar quantitative results (Figure S25). The only noticeable difference regards the O1s peak, whose shape is influenced by the absorption of hydroxyl groups due to the alkaline solution employed in the photoelectrochemical tests (see component O_2 in Figures 3 and S8, located at 531.5 eV), as presented in Figure S24c. Such results indicate that the obtained materials are not appreciably altered after prolonged usage even in seawater, an important pre-requisite in view of eventual large-scale applications.

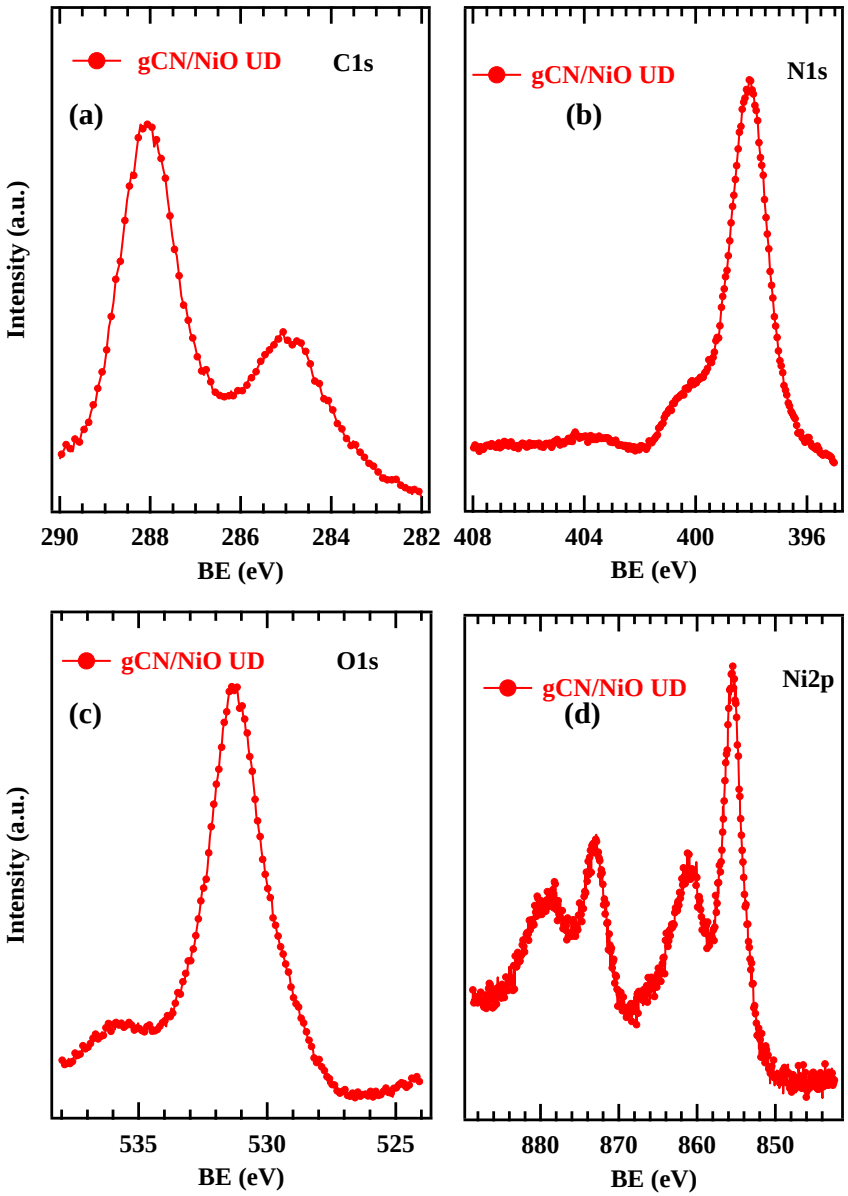

Figure S24. XPS analysis for specimen gCN/NiO UD after completion of the tests indicated in Figure S23 and a final further test in Adriatic alkaline seawater (pH = 13.58).

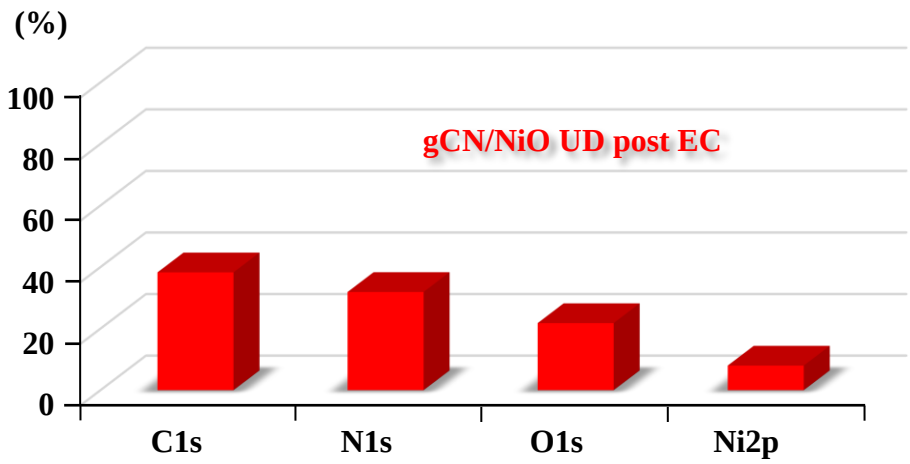

Figure S25. Atomic percentage (at. %) data obtained by XPS analyses for specimen gCN/NiO UD after completion of the tests indicated in Figure S23 and a final further test in Adriatic alkaline seawater (pH = 13.58).

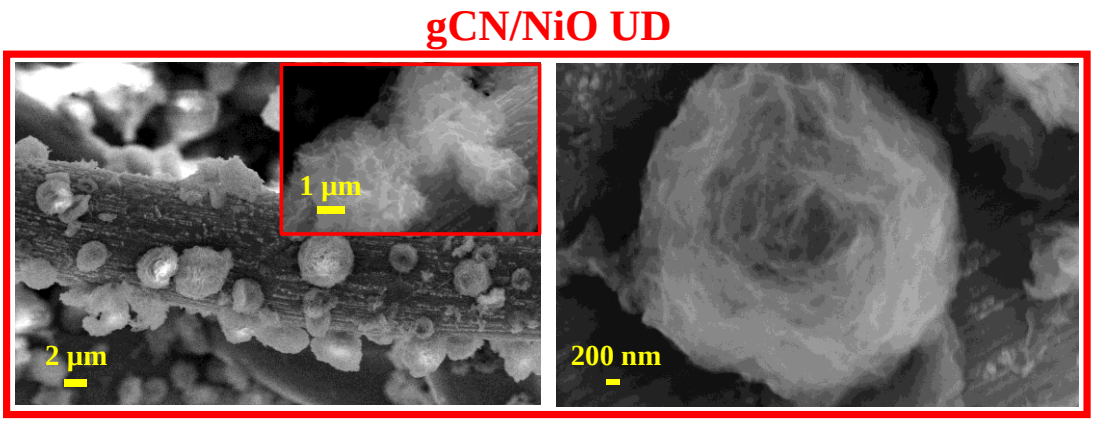

Figure S26. Representative FE-SEM micrographs for sample gCN/NiO UD after completion of the tests indicated in Figure S23 and a final further test in Adriatic alkaline seawater (pH = 13.58).

§ S5. References

[1] M. I. Chebanenko, A. A. Lobinsky, V. N. Nevedomskiy, V. I. Popkov, *Dalton Trans.* **2020**, *49*, 12088-12097.

[2] Y. Wang, X. Li, R. Zhao, N. Zhang, B. Zhu, J. Yang, *Appl. Surf. Sci.* **2020**, *532*, 147410.

[3] S. Zhang, J. Yan, S. Yang, Y. Xu, X. Cai, X. Li, X. Zhang, F. Peng, Y. Fang, *Chin. J. Catal.* **2017**, *38*, 365-371.

[4] L. Besra, M. Liu, *Prog. Mater. Sci.* **2007**, *52*, 1-61.

[5] M. Benedet, A. Gallo, C. Maccato, G. A. Rizzi, D. Barreca, O. I. Lebedev, E. Modin, R. McGlynn, D. Mariotti, A. Gasparotto, *ACS Appl. Mater. Interfaces* **2023**, *15*, 47368-47380.

[6] a) M. Benedet, G. A. Rizzi, A. Gasparotto, O. I. Lebedev, L. Girardi, C. Maccato, D. Barreca, *Chem. Eng. J.* **2022**, *448*, 137645; b) M. Benedet, G. A. Rizzi, A. Gasparotto, N. Gauquelin, A. Orekhov, J. Verbeeck, C. Maccato, D. Barreca, *Appl. Surf. Sci.* **2023**, *618*, 156652.

[7] I. Bertóti, M. Mohai, K. László, *Carbon* **2015**, *84*, 185-196.

[8] G. Pagot, M. Benedet, C. Maccato, D. Barreca, V. Di Noto, *Surf. Sci. Spectra* **2023**, *30*, 024028.

[9] I. Preda, R. J. O. Mossanek, M. Abbate, L. Alvarez, J. Méndez, A. Gutiérrez, L. Soriano, *Surf. Sci.* **2012**, *606*, 1426-1430.

[10] M. A. Peck, M. A. Langell, *Chem. Mater.* **2012**, *24*, 4483-4490.

[11] a) Y. Fu, C. a. Liu, C. Zhu, H. Wang, Y. Dou, W. Shi, M. Shao, H. Huang, Y. Liu, Z. Kang, *Inorg. Chem. Front.* **2018**, *5*, 1646-1652; b) K. Qi, A. Zada, Y. Yang, Q. Chen, A. Khataee, *Res. Chem. Intermed.* **2020**, *46*, 5281-5295; c) X. Li, H. Zhang, Y. Liu, X. Duan, X. Xu, S. Liu, H. Sun, S. Wang, *Chem. Eng. J.* **2020**, *390*, 124634.

[12] J. Zhu, L. Kong, X. Shen, G. Zhu, Z. Ji, K. Xu, H. Zhou, X. Yue, B. Li, *J. Electroanal. Chem.* **2020**, *873*, 114390.

[13] J.C. Alexander, *Surface modifications and growth of titanium dioxide for photo-electrochemical water splitting*; Springer Theses, 2016.

[14] a) M. Benedet, G. A. Rizzi, O. I. Lebedev, V. Roddatis, C. Sada, J.-L. Wree, A. Devi, C. Maccato, A. Gasparotto, D. Barreca, *J. Mater. Chem. A* **2023**, *11*, 21595-21609; b) D. Barreca, G. Carraro, A. Gasparotto, C. Maccato, M. E. A. Warwick, K. Kaunisto, C. Sada, S. Turner, Y. Gönüllü, T.-P. Ruoko, L. Borgese, E. Bontempi, G. Van Tendeloo, H. Lemmetyinen, S. Mathur, *Adv. Mater. Interfaces* **2015**, *2*, 1500313.

[15] R. Wang, K. Pan, D. Han, J. Jiang, C. Xiang, Z. Huang, L. Zhang, X. Xiang, *ChemSusChem* **2016**, *9*, 2470-2479.

[16] Z. Chen, H. Wang, J. Xu, J. Liu, *Chem. Asian J.* **2018**, *13*, 1539-1543.

[17] G. Zhang, S. Zang, X. Wang, *ACS Catal.* **2015**, *5*, 941-947.

[18] H. Wang, T. Sun, L. Chang, P. Nie, X. Zhang, C. Zhao, X. Xue, *Electrochim. Acta* **2019**, *303*, 110-117.

[19] S. Ohn, S. Y. Kim, S. K. Mun, J. Oh, Y. J. Sa, S. Park, S. H. Joo, S. J. Kwon, S. Park, *Carbon* **2017**, *124*, 180-187.

[20] J. Yan, H. Wu, H. Chen, L. Pang, Y. Zhang, R. Jiang, L. Li, S. Liu, *Appl. Catal., B* **2016**, *194*, 74-83.

[21] S. F. Blaskievicz, H. L. S. Santos, I. F. Teixeira, J. L. Bott-Neto, P. S. Fernández, L. H. Mascaro, *Mater. Today Nano* **2022**, *18*, 100192.

[22] K. Bhunia, S. Khilari, M. Chandra, D. Pradhan, S.-J. Kim, *J. Alloys Compd.* **2023**, *935*, 167842.

[23] P. Chaudhary, P. P. Ingole, *Int. J. Hydrogen Energy* **2020**, *45*, 16060-16070.

[24] M. Shakeel, M. Arif, G. Yasin, B. Li, H. D. Khan, *Appl. Catal., B* **2019**, *242*, 485-498.

[25] W. Zhang, J. Albero, L. Xi, K. M. Lange, H. Garcia, X. Wang, M. Shalom, *ACS Appl. Mater. Interfaces* **2017**, *9*, 32667-32677.

[26] P. Longchin, D. Mitoraj, O. M. Reyes, C. Adler, N. Wetchakun, R. Beranek, *J. Phys.: Energy* **2020**, *2*, 044001.

[27] L. Jiao, Y.-X. Zhou, H.-L. Jiang, *Chem. Sci.* **2016**, *7*, 1690-1695.

[28] U. Y. Qazi, C. Z. Yuan, N. Ullah, Y. F. Jiang, M. Imran, A. Zeb, S. J. Zhao, R. Javaid, A. W. Xu, *ACS Appl. Mater. Interfaces* **2017**, *9*, 28627-28634.

[29] H. Sim, J. Lee, T. Yu, B. Lim, *Korean J. Chem. Eng.* **2018**, *35*, 257-262.

[30] Q. Xiao, Y. Zhang, X. Guo, L. Jing, Z. Yang, Y. Xue, Y.-M. Yan, K. Sun, *Chem. Commun.* **2014**, *50*, 13019-13022.

[31] D. Das, A. Das, M. Reghunath, K. K. Nanda, *Green Chem.* **2017**, *19*, 1327-1335.

[32] M. S. Ahmed, B. Choi, Y.-B. Kim, *Sci. Rep.* **2018**, *8*, 2543.

[33] T. Li, X. Ma, J. Wu, F. Chu, L. Qiao, Y. Song, M. Wu, J. Lin, L. Peng, Z. Chen, *Electrochim. Acta* **2021**, *400*, 139473.